CHEMISTRY OF MATERIALS
Article

Chem. Mater. **2009,** *21,* 4515–4526 4515
DOI:10.1021/cm901203n

Highly Stable and Active Pt−Cu Oxygen Reduction Electrocatalysts Based on Mesoporous Graphitic Carbon Supports

Gaurav Gupta,[†] Daniel A. Slanac,[†] Pavan Kumar,[†] Jaclyn D. Wiggins-Camacho,[†] Xiqing Wang,[‡] Steven Swinnea,[†] Karren L. More,[‡] Sheng Dai,[‡] Keith J. Stevenson,[†] and Keith P. Johnston*[,†]

[†]*University of Texas at Austin, 1 University Station C0400, Austin, Texas 78712, and* [‡]*Oak Ridge National Laboratories, 1 Bethel Valley Road, Oak Ridge, Tennessee 37831*

Received May 8, 2009. Revised Manuscript Received July 9, 2009

The activity of oxygen reduction catalysts for fuel cells often decreases markedly (30−70%) during potential cycling tests designed to accelerate catalyst degradation. Herein we achieved essentially no loss in electrochemical surface area and catalyst activity during potential cycling from 0.5 to 1.2 V for presynthesized Pt−Cu nanoparticles of controlled composition that were infused into highly graphitic disordered mesoporous carbons (DMC). The high stability is favored by the strong metal−support interactions and low tendency for carbon oxidation, which mitigates the mechanisms of degradation. Electrochemical dealloying transforms the composition from $Pt_{20}Cu_{80}$ to $Pt_{85}Cu_{15}$ with a strained Pt-rich shell, which exhibits an enhanced ORR activity of 0.46 A/mg_{Pt}, > 4 fold that of pure Pt catalysts. The high uniformity in particle size and composition both before and after dealloying, as a consequence of the presynthesis/infusion technique, is beneficial for elucidating the mechanism of catalyst activity and, ultimately, for designing more active catalysts.

Introduction

The successful commercialization of polymer electrolyte membrane fuel cells (PEMFC) depends upon: (1) a significant increase in electrocatalytic mass activity > 4 times that of pure Pt for the oxygen reduction reaction (ORR)[1−5] and (2) catalyst stability against potential cycling designed to simulate fuel cell operating conditions over the catalyst lifetime.[6] Recently, the activity of Pt-based catalyst has improved by a factor of about 2.5 using Pt alloyed with another metal (i.e. Pt-M, where M = Co, Ni, Fe, V, Ti).[2,4,7−12] Furthermore, Strasser and co-workers synthesized novel Pt−Cu catalysts on activated carbon supports that exhibited pronounced activity enhancements of > 4 times that of pure Pt catalysts.[1,13] The highly active ORR catalysts were prepared by electrochemically dealloying Cu to create a strained Pt shell[1,13−17] with a shorter Pt−Pt distance. The strain lowers the d-band centers relative to the Fermi level and consequently enhances the ORR activity according to DFT studies.[18−20] The resulting reduction in the adsorption energy of oxygen and coverage of Pt surface sites by oxygen intermediate species[4] enhances the activity.

The stability of Pt-based ORR catalysts is also a major concern. Pt catalysts supported on carbon can experience several degradation mechanisms when subjected to extreme potential cycling, mimicking the harsh environment in a

---

*Corresponding author. E-mail: kpj@che.utexas.edu.

(1) Koh, S.; Strasser, P. *J. Am. Chem. Soc.* **2007**, *129*(42), 12624–12625.
(2) Stamenkovic, V. R.; Fowler, B.; Mun, B. S.; Wang, G.; Ross, P. N.; Lucas, C. A.; Markovic, N. M. *Science* **2007**, *315*(5811), 493–497.
(3) Zhang, J.; Lima, F. H. B.; Shao, M. H.; Sasaki, K.; Wang, J. X.; Hanson, J.; Adzic, R. R. *J. Phys. Chem. B* **2005**, *109*(48), 22701–22704.
(4) Stamenkovic, V. R.; Mun, B. S.; Arenz, M.; Mayrhofer, K. J. J.; Lucas, C. A.; Wang, G.; Ross, P. N.; Markovic, N. M. *Nat. Mater.* **2007**, *6*(3), 241–247.
(5) Gasteiger, H. A. *Electrochemistry* **2007**, *75*(2), 103.
(6) Wagner, F. T.; Gasteiger, H. A.; Makharia, R.; Neyerlin, K. C.; Thompson, E. L.; Yan, S. G. *ECS Trans.* **2006**, *3*(1, Proton Exchange Membrane Fuel Cells 6), 19–29.
(7) Salgado, J. R. C.; Antolini, E.; Gonzalez, E. R. *J. Phys. Chem. B* **2004**, *108*(46), 17767–17774.
(8) Koh, S.; Leisch, J.; Toney, M. F.; Strasser, P. *J. Phys. Chem. C* **2007**, *111*(9), 3744–3752.
(9) Xiong, L.; Manthiram, A. *Electrochim. Acta* **2005**, *50*(11), 2323–2329.
(10) Xiong, L.; Manthiram, A. *J. Electrochem. Soc.* **2005**, *152*(4), A697–A703.
(11) Wakabayashi, N.; Takeichi, M.; Uchida, H.; Watanabe, M. *J. Phys. Chem. B* **2005**, *109*(12), 5836–5841.
(12) Yano, H.; Kataoka, M.; Yamashita, H.; Uchida, H.; Watanabe, M. *Langmuir* **2007**, *23*(11), 6438–6445.
(13) Mani, P.; Srivastava, R.; Strasser, P. *J. Phys. Chem. C* **2008**, *112*(7), 2770–2778.
(14) Mani, P.; Srivastava, R.; Yu, C.; Strasser, P. *ECS Trans.* **2007**, *11*(1, Part 2, Proton Exchange Membrane Fuel Cells 7, Part 2), 933–939.
(15) Strasser, P.; Koh, S.; Yu, C. *ECS Trans.* **2007**, *11*(1, Part 1, Proton Exchange Membrane Fuel Cells 7, Part 1), 167–180.
(16) Koh, S.; Yu, C.; Strasser, P. *ECS Trans.* **2007**, *11*(1, Part 1, Proton Exchange Membrane Fuel Cells 7, Part 1), 205–215.
(17) Yu, C.; Koh, S.; Leisch, J. E.; Toney, M. F.; Strasser, P. *Faraday Discuss.* **2008**, *140*, 283–296.
(18) Xu, Y.; Ruban, A. V.; Mavrikakis, M. *J. Am. Chem. Soc.* **2004**, *126* (14), 4717–4725.
(19) Greeley, J.; Krekelberg, W. P.; Mavrikakis, M. *Angew. Chem., Int. Ed.* **2004**, *43*(33), 4296–4300.
(20) Schlapka, A.; Lischka, M.; Gross, A.; Kasberger, U.; Jakob, P. *Phys. Rev. Lett.* **2003**, *91*(1), 016101/1–016101/4.
(21) Zhang, J.; Sasaki, K.; Sutter, E.; Adzic, R. R. *Science* **2007**, *315* (5809), 220–222.
(22) Wang, J.; Yin, G.; Shao, Y.; Wang, Z.; Gao, Y. *J. Phys. Chem. C* **2008**, *112*(15), 5784–5789.
(23) Shao, Y.; Yin, G.; Gao, Y.; Shi, P. *J. Electrochem. Soc.* **2006**, *153* (6), A1093–A1097.
(24) Ferreira, P. J.; la O, G. J.; Shao-Horn, Y.; Morgan, D.; Makharia, R.; Kocha, S.; Gasteiger, H. A. *J. Electrochem. Soc.* **2005**, *152*(11), A2256–A2271.

PEMFC (e.g. in transportation applications).[21−24] For Pt supported on traditional amorphous carbons, significant losses in activity occur via carbon oxidation as well as Pt dissolution/redeposition processes. For Pt supported on Vulcan XC-72 carbon, the electrochemical surface area decreases ~70% after potential cycling between 0.5 V and 1.2 V for 1000 cycles.[25] Excellent stability has been shown for a PtCu catalyst over potential cycling from 0.5 to 1.0 V for 30 000 cycles.[26] However, the solubility of Pt ions increases substantially above 1.1 V (potentials which can be seen in at open circuit potential for idle automotive fuel cells). In addition, by limiting the lower potential to 0.5 V, the βPt oxide is not reduced to Pt, further accelerating the Pt degradation.[25]

Oxidation of the carbon support weakens the Pt−support interactions and enhances Pt dissolution/redeposition and agglomeration.[27] Carbons with a higher level of graphitization have shown improved resistance to oxidation.[27−29] In addition, several studies have indicated that the abundant π electron sites in graphite interact more strongly with Pt via electron delocalization and charge transfer, as supported by XPS and electron-spin resonance (ESR) data.[27−30] The strong electronic metal−support interactions may also inhibit Pt oxidation and dissolution during potential cycling and lower the degree of Ostwald ripening and coalescence.[28] Thus, oxidation resistant graphitic supports with strong catalyst−support interactions are expected to provide substantial improvement in stability and durability for ORR. Recently, Pt particles have been successfully dispersed on graphitic mesoporous carbon with an organic impregnation method and have shown enhanced stability during potential cycling from 0.0 to 1.0 V for 160 h.[31]

Though graphitic supports offer potential stability advantages, metals such as Pt are not dispersed efficiently on graphitic carbon upon reduction of ionic precursors, for example, in the wetness impregnation technique.[28,32,33] The ionic precursors often interact too weakly with graphitized supports, which do not have a sufficient number of polar surface oxygen sites. To form bimetallic catalysts, we must reduce multiple metal precursors on the supports either simultaneously[34,35] or sequentially.[1,36] These approaches often produce nanoparticles with high polydispersity in size and multiple alloy phases.[37] The lack of homogeneity results from nonuniform interactions with the heterogeneous support as well as varying rates of nucleation and growth for each metal precursor in solution.[13,14]

An emerging concept in catalyst design is the presynthesis of metal nanocrystals with controlled size and composition via arrested growth precipitation with stabilizing ligands followed by infusion of these nanocrystals onto high-surface-area supports.[38−44] Arrested growth precipitation provides much greater control over the nanocrystal size, composition, and alloy structure than traditional techniques where reduction in the presence of the support complicates nucleation, growth, and binding of stabilizing ligands. Weakly bound low-molecular-weight ligands have been designed to stabilize the nanocrystals while exposing significant metal area to the support for sufficient binding to achieve loading up to 15 wt %.[40,41] The ligands may be removed at low temperatures to activate the catalyst without perturbing the nanocrystal structure significantly.

The primary objective of this study was to prepare highly stable and active ORR catalysts by supporting Pt−Cu catalysts on mesoporous graphitic carbons. We demonstrate that high surface area (> 300 m^2/g), oxidation-resistant, graphitic mesoporous carbon supports, which bind to Pt[28] as well as copper,[45] mitigate nanoparticle coalescence, metal dissolution, and Ostwald ripening during potential cycling. The potential was cycled between 0.5 and 1.2 V for 1000 cycles at 50 mV/s to perform an accelerated durability test. The Pt−Cu nanoparticles were presynthesized by arrested growth precipitation to control the size and achieve high uniformity in alloy composition. They were then infused into disordered mesoporous carbons with large pore size (~8 nm) to achieve high dispersion. Weakly binding ligands (oleic acid and oleylamine) were chosen to expose a significant fraction of the copper-rich surface domains to the graphitic π sites to promote strong metal−support interactions and to allow removal via calcination at low temperatures (~350 °C) to activate the catalyst. The nanoparticles were subsequently electrochemically dealloyed to selectively remove Cu to form a strained Pt shell for the enhancement of the catalyst activity, as reported previously.[1,13] The dealloying produced essentially a single phase, $Pt_{85}Cu_{15}$. The degree of graphitization of the mesoporous carbons (without metal) was characterized

---

(25) Waje, M. M.; Li, W.; Chen, Z.; Larsen, P.; Yan, Y. *ECS Trans.* **2007**, *11*(1, Part 2, Proton Exchange Membrane Fuel Cells 7, Part 2), 1227–1233.
(26) Neyerlin, K. C.; Srivastava, R.; Yu, C.; Strasser, P. *J. Power Sources* **2009**, *186*(2), 261–267.
(27) Coloma, F.; Sepulveda-Escribano, A.; Rodriquez-Reinoso, F. *J. Catal.* **1995**, *154*(2), 299–305.
(28) Yu, X.; Ye, S. *J. Power Sources* **2007**, *172*(1), 145–154.
(29) Shao, Y.; Yin, G.; Gao, Y. *J. Power Sources* **2007**, *171*(2), 558–566.
(30) Cuong, N. T.; Chi, D. H.; Kim, Y.-T.; Mitani, T. *Phys. Status Solidi* **2006**, *13*, 3472–3475.
(31) Shanahan, P. V.; Xu, L.; Liang, C.; Waje, M.; Dai, S.; Yan, Y. S. *J. Power Sources* **2008**, *185*(1), 423–427.
(32) Yu, X.; Ye, S. *J. Power Sources* **2007**, *172*(1), 133–144.
(33) Wakayama, H.; Setoyama, N.; Fukushima, Y. *Adv. Mater.* **2003**, *15*(9), 742–745.
(34) Raghuveer, V.; Ferreira, P. J.; Manthiram, A. *Electrochem. Commun.* **2006**, *8*(5), 807–814.
(35) Freund, A.; Lang, J.; Lehmann, T.; Starz, K. A. *Catal. Today* **1996**, *27*(1−2), 279–83.
(36) Min, M.-K.; Cho, J.; Cho, K.; Kim, H. *Electrochim. Acta* **2000**, *45* (25−26), 4211–4217.
(37) Antolini, E. *Mater. Chem. Phys.* **2003**, *78*(3), 563–573.
(38) Rioux, R. M.; Song, H.; Hoefelmeyer, J. D.; Yang, P.; Somorjai, G. A. *J. Phys. Chem. B* **2005**, *109*(6), 2192–2202.
(39) Gupta, G.; Shah, P. S.; Zhang, X.; Saunders, A. E.; Korgel, B. A.; Johnston, K. P. *Chem. Mater.* **2005**, *17*(26), 6728–6738.
(40) Gupta, G.; Stowell, C. A.; Patel, M. N.; Gao, X.; Yacaman, M. J.; Korgel, B. A.; Johnston, K. P. *Chem. Mater.* **2006**, *18*, 6239–6249.
(41) Gupta, G.; Patel, M. N.; Ferrer, D.; Heitsch, A. T.; Korgel, B. A.; Johnston, K. P. *Chem. Mater.* **2008**, *20*, 5005–5015.
(42) Chen, Y.; Yang, F.; Dai, Y.; Wang, W.; Chen, S. *J. Phys. Chem. C* **2008**, *112*(5), 1645–1649.
(43) Vijayaraghavan, G.; Stevenson, K. J. *Langmuir* **2007**, *23*(10), 5279–5282.
(44) Ye, H.; Crooks, R. M. *J. Am. Chem. Soc.* **2007**, *129*(12), 3627–3633.
(45) Hou, J. G.; Li, X.; Wang, H.; Wang, B. *J. Phys. Chem. Solids* **2000**, *61*(7), 995–998.

by XRD and Raman spectroscopy and the oxidative stability in the presence of Pt by thermal gravimetric analysis. In addition, the size and composition of Pt−Cu nanoparticles were characterized before and after electrochemical dealloying by TEM, XRD and SEM-EDS to provide insight into the activity and stability for the ORR reaction and the stability under potential cycling.

Experimental Section

All chemicals were used as received. Platinum(II) acetylacetonate (97%), copper bis(2,2,6,6-tetramethyl-3,5-heptanedionate), oleylamine (70%), oleic Acid (99%) diphenyl ether (98% purity), perchloric acid 70% (99.999% purity), anhydrous ethanol, and 5 wt % nafion solution in lower alcohols were purchased from Aldrich. Toluene (99.9%) was obtained from Fisher Scientific, and ethanol (Absolute 200 proof) from Aaper alcohol. Polycarbonate filters (0.05 μm) were obtained from Osmonics. High purity water (resistance ~ 18 MΩ) was used. Oxygen (research grade, 99.999% purity) and argon (research grade, 99.999% purity) were obtained from Praxair.

Pt−Cu Nanoparticle Synthesis. Pt−Cu particles were synthesized by employing the modified polyol process described by Sun et al.[46] The synthesis was carried out in a 50 mL three-neck flask under an argon atmosphere using standard Schlenk line techniques. For the preparation of $Pt_{20}Cu_{80}$ nanoparticles, 0.16 mmol of platinum acetylacetonate and 0.50 mmol of copper bis(2,2,6,6-tetramethyl-3,5-heptanedionate) were separately dissolved in 10 mL of diphenyl ether and injected into the flask. The solution was continuously stirred and heated to 80 °C using a heating mantle. At 80 °C, 0.5 mmol of the stabilizing agents, oleic acid and oleyl amine, were injected. The temperature was then raised to the reflux temperature of diphenyl ether (~260 °C). At around 215 °C, a sudden change in the reaction mixture was observed as the solution turned yellow and then dark brown, indicating the reduction of the precursors. The reaction mixture was maintained at 260 °C for 30 min and then cooled to room temperature. The dark dispersion was removed from the flask and the particles were isolated by the addition of 50 mL of acetone and centrifugation. The nanoparticles were further cleaned by redispersing the $Pt_{20}Cu_{80}$ particles in 1 mL of toluene and excess acetone and centrifuging again. The other compositions of Pt−Cu were synthesized by changing the molar ratios of the precursors.

Mesoporous Carbon Synthesis. Disordered mesoporous carbons (DMC) were prepared via self-assembly of block copolymer and phenolic resin under acidic conditions as described in our previous reports.[47,48] Typically, 16.5 g of resorcinol and 16.5 g of F127 ($EO_{106}PO_{70}EO_{106}$) were dissolved in 67.5 mL of EtOH and 67.5 mL of HCl aqueous solution (3.0 M). To this solution was added 19.5 g of formaldehyde (37 wt % in H2O) with stirring at room temperature. As the polymerization reaction of resorcinol and formaldehyde proceeded, self-assembly of in situ formed phenolic resin and F127 induced a phase separation. The polymer-rich gel phase was collected in the bottom of centrifuge tubes by centrifugation at 9500 rpm for 4 min after the mixture was stirred for 30 min. The gel was dissolved in a mixed solvent of 18 g of THF and 12 g of EtOH and the mixture was loaded on a substrate, dried at room temperature overnight, and cured at 80 °C for 24 h. Carbonization was carried out under a N_2 atmosphere at 400 °C for 2 h with a heating rate of 1 °C/min, which was followed by further treatment at 850 °C for 3 h with a heating rate of 5 °C/min. To enhance the degree of graphitization, the heat treatment of mesoporous carbons was carried out in a high-temperature furnace (Thermal Technology Inc., CA) under helium atmosphere at desired temperatures for 1 h with a heating ramp of 20 °C/min. The mesoporous carbons heat-treated at temperatures of 850, 2000, and 2600 °C will be referred to as DMC-850, DMC-2000, and DMC-2600, respectively, for the rest of the article. The conductivity of the DMC-2000 and DMC-2600 is ~ 300 S/cm, about 2 orders of magnitude higher than that of Vulcan XC-72 carbon.[49] The conductivity of the less graphitic DMC-850 is only 2.0 S/cm. The pores of the mesoporous carbons were disordered in nature as peaks were not present in small-angle X-ray scattering (not shown).

Infusion of Pt−Cu Nanoparticles into Mesoporous Carbon. The infusion of the Pt−Cu nanoparticles into mesoporous carbon was done by a similar procedure as reported by Gupta et al.[41] Twenty-five milligrams of mesoporous carbon was mixed with 3 mL of a Pt−Cu nanocrystal dispersion of known concentration, ~20 mg/mL, in toluene. The contents were stirred for 4 days. The product was separated from the nanocrystal supernatant by filtration with a 0.2 μm PTFE filter. The extent of incorporation of Pt−Cu nanocrystals in the carbon was determined by subtracting from the initial mass of Pt−Cu in toluene, the final mass recovered in the supernatant after filtration.[39] The masses were determined by absorbance of the Pt−Cu nanocrystals with a Cary 500 UV−vis−NIR spectrophotometer with an optical path length of 1 cm (see Figure S3 in the Supporting Information). A standard linear calibration curve was generated with known concentrations of Pt−Cu nanocrystals in toluene for a wavelength of 800 nm with correlation coefficient of 0.998 (Figure S3). Loadings of ~15% metal on mesoporous carbons were obtained after infusion (Table 2). The individual uncertainties in the loadings are (±2%), (±1%), (±1%), and (±3%), respectively, resulting from uncertainties in volume, mass of carbon, absorbance, and linearity of the calibration curve. The total uncertainty is calculated conservatively by adding the individual uncertainties in loadings and is ~7%, as explained in detail previously.[40] To activate the Pt−Cu catalysts ligands were removed by calcining the catalyst at 350 °C for 2 h. The temperature was ramped at 16 °C/min. After calcination, the catalysts were washed with 100 mL of ethanol.

X-ray Diffraction. Wide-angle X-ray diffraction was performed with samples on a quartz slide using a Bruker-Nonius D8 Advance diffractometer. Samples were scanned for 12 h at a scan rate of 12°/min with 0.02° increments. The average nanocrystal size was estimated from the Scherrer equation using JADE software (by Molecular Diffraction Inc.). Peak deconvolutions were done using JADE software. All of the fits were background-corrected (cubic spline method) and the carbon intensity was subtracted.

Raman Analysis. Raman spectra were acquired using a Renishaw inVia Microscope using a 514.5 nm Argon laser at 50% power with a 50x aperture. Four acquisitions were taken for each sample from 500 to 2000 cm^{-1} for 50 s. The spectra were fit using the PeakFit software, following the convention set forth by Cuesta et al.[50] of fitting five Gaussians at 1624, 1583, 1487, 1351, and 1220 cm^{-1}, corresponding to the D′, G, D″, D, and

---

(46) Sun, X.; Kang, S.; Harrell, J. W.; Nikles, D. E.; Dai, Z. R.; Li, J.; Wang, Z. L. *J. Appl. Phys.* **2003**, *93*(10, Pt. 2), 7337–7339.

(47) Liang, C.; Dai, S. *J. Am. Chem. Soc.* **2006**, *128*(16), 5316–5317.

(48) Wang, X.; Liang, C.; Dai, S. *Langmuir* **2008**, *24*(14), 7500–7505.

(49) Pantea, D.; Darmstadt, H.; Kaliaguine, S.; Summchen, L.; Roy, C. *Carbon* **2001**, *39*(8), 1147–1158.

(50) Cuesta, A.; Dhamelincourt, P.; Laureyns, J.; Martinez-Alonso, A.; Tascon, J. M. D. *Carbon* **1994**, *32*(8), 1523–32.

Table 1. Properties of Mesoporous Carbon

carbon	surface area (m^2/g)	pore volume	pore size (nm)	L_a (Å)	L_c (Å)	*d* (Å)
DMC 850	577	0.70	8.1	33.8	16	3.81
DMC 2000	344	0.57	8.0	35.4	22	3.63
DMC 2600	262	0.39	7.9	43.2	30	3.35

Table 2. Infusion of Pt−Cu Nanoparticles in Mesoporous Carbon Supports[a]

nano-particles	support	time of infusion (days)	initial conc. (mg/mL)	final conc. (mg/mL)	loading (wt %)
$Pt_{20}Cu_{80}$	DMC-850	3	20	15.5	17
$Pt_{20}Cu_{80}$	DMC-2000	3	20	18	8
$Pt_{20}Cu_{80}$	DMC-2000	5	30	26	14
$Pt_{45}Cu_{55}$	DMC-2600	7	30	26	14
$Pt_{20}Cu_{80}$	Vulcan-XC72	2	5	< 0.1	19

[a] All infusions were done on 50 mg of carbon and nanoparticles were dispersed in 3 mL of toluene. The infusion times and concentrations were increased in order to achieve high loadings.

I bands, respectively. All spectral fits had correlation factors (R^2) greater than 0.98.

Electrochemical Apparatus. A glassy carbon rotating disk electrode (0.196 cm^2, from Pine Instruments) was used as the working electrode. It was polished with a 0.3 μm followed by a 0.05 μm alumina suspension to give a mirror finish. 1.0 mg of Pt−Cu catalyst was suspended by sonication in 300 μL of anhydrous ethanol and 300 μL of 0.15 wt % nafion solution (diluted from 5% nafion stock solution). A total of 10 μL of Pt−Cu suspension was pipetted onto the substrate and was dried at room temperature for 15 min.

Electrochemical measurements were carried out using a three-compartment electrochemical cell with a Pt wire counter electrode and a Hg/Hg_2SO_4 reference electrode. Electrochemical measurements were recorded using CHI 832 electrochemical analyzer (CH instruments Inc., Austin). All potentials cited in this article are normalized with respect to NHE.

Electrochemical Measurements. All experiments were performed at room temperature. After preparation of the catalyst on the substrate, the catalyst was electrochemically dealloyed to preferentially remove Cu by cycling the potential between 0.05 and 1.24 V at 200 mV/s for 500 cycles in argon saturated 0.1 M $HClO_4$ electrolyte.[1] The area under the desorption peak of underpotentially deposited hydrogen in a cyclic voltammogram (scanned at 100 mV/s between 0.04 and 1.24 V), was used to evaluate electrochemically active surface area (ECSA) of the Pt catalyst on the electrode. Hydrodynamic voltammograms at rotating disk electrode were recorded by anodically scanning the potential from 0.04 to 1.24 V at 5 mV/s in oxygen saturated 0.1 M $HClO_4$. The oxygen pressure was 1 atm. All mass and specific activities were calculated at a current at 0.9 V vs NHE from the hydrodynamic voltammograms, given the known mass and area of Pt. Accelerated durability tests (ADT) were employed by cycling the electrode potential between 0.5 and 1.2 V at 50 mV/s for 1000 cycles in an argon saturated atmosphere for a total time of 7 h.[25]

Additional Structural Characterization. For details on porosimetry, TEM, SEM, and XPS see the Supporting Information.

Results

Structure of the Pt−Cu−mesoporous Carbon Catalysts. The surface area, pore volume and mean pore size for the three carbons measured by nitrogen porosimetry (see the Supporting Information) are given in Table 1. As the calcination temperature for the carbons increases from 850 to 2600 °C, both the surface area and the pore volume decrease as expected. DMC-850 and DMC-2000 have surface areas of 577 and 344 m^2/g respectively, which are significantly higher than that of commercial Vulcan XC-72 (~250 m^2/g) supports. The pore size for all three mesoporous carbons was ~8 nm, indicating lack of structural collapse even at the highest calcination temperature.

XRD spectra of the carbons annealed at various temperatures are shown in Figure 1A. The peak at ~25° corresponds to the ⟨002⟩ plane of graphite. A sharp ⟨002⟩ peak is associated with a higher graphitic character as compared to a broad diffuse peak seen in amorphous carbons.[51] With increasing annealing temperature, the ⟨002⟩ peak becomes sharper and narrower, indicating an increase in the degree of graphitization. The layer dimension parallel to the basal place, L_a, and perpendicular, L_c, were calculated from the ⟨100⟩ and ⟨002⟩ reflections, respectively, according the relations,[51,52] $L_a = 1.84\lambda/B\cos(\theta)$ and $L_c = 0.89\lambda/B\cos(\theta)$, where λ is the wavelength of the X-rays (1.54A), B is the full angular width at half max, and θ is the Bragg angle (Table 1). The monotonic increase in the values of L_a and L_c with increasing temperature indicates progressive graphitization of the carbon supports. Table 1 also lists the interplanar *d*-spacing calculated from the ⟨002⟩ reflection using Bragg's law, $n\lambda = 2d\sin(\theta)$. The monotonic decrease in *d*-spacing toward that of pure graphite as the annealing temperature is increased further indicates increasing graphitization.[51] The *d*-spacing from XRD corresponds well with that measured from the high resolution TEM image of DMC 2000 in Figure 1B (3.63 Å). Layered ribbon-like graphitic structures are evident. The black lines in the layers are individual graphene planes. The significant amount of graphite ribbons in the carbon is consistent with the sharp ⟨002⟩ peak observed for DMC 2000.

The first order Raman spectra for DMC-850, 2000, and 2600 are shown in Figure 2. There are two peaks apparent in the spectra for all three samples, corresponding to the D band at 1355 cm^{-1} and the G band at 1583 cm^{-1}. Increasing the annealing temperature for the carbons enhances the overlap between the two bands, making it necessary to deconvolute the fwhm values by fitting five bands at 1624, 1583, 1487, 1355, and 1220 cm^{-1}, corresponding to the D′, G, D″, D, and I bands, respectively, following the convention of Cuesta et al.[50] The D band is often referred to as the "disorder" band and is commonly believed to be a Raman inactive mode that becomes active as the disorder in the system is increased, or likewise as the symmetry at or near a crystalline edge is reduced.[53,54]

---

(51) Kinoshita, K. *Carbon: Electrochemical and Physicochemical Properties*. John Wiley and Sons: New York, 1988.

(52) Tian, J. M.; Wang, F. B.; Shan, Z. H. Q.; Wang, R. J.; Zhang, J. Y. *J. Appl. Electrochem.* **2004**, *34*(5), 461–467.

(53) Nemanich, R. J.; Solin, S. A. *Phys. Rev. B: Condens. Matter Mater. Phys.* **1979**, *20*(2), 392–401.

(54) Maldonado, S.; Morin, S.; Stevenson, K. J. *Carbon* **2006**, *44*(8), 1429–1437.

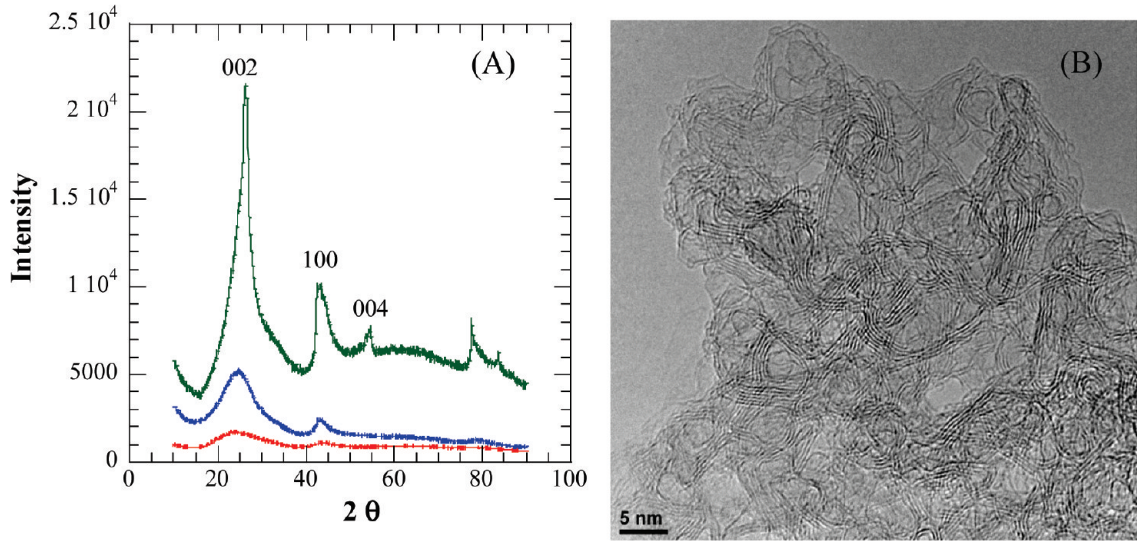

Figure 1. (A) XRD spectra of the disordered mesoporous carbons annealed at different temperatures; (B) high-resolution TEM of DMC 2000 with a measured *d*-spacing of 3.63 Å.

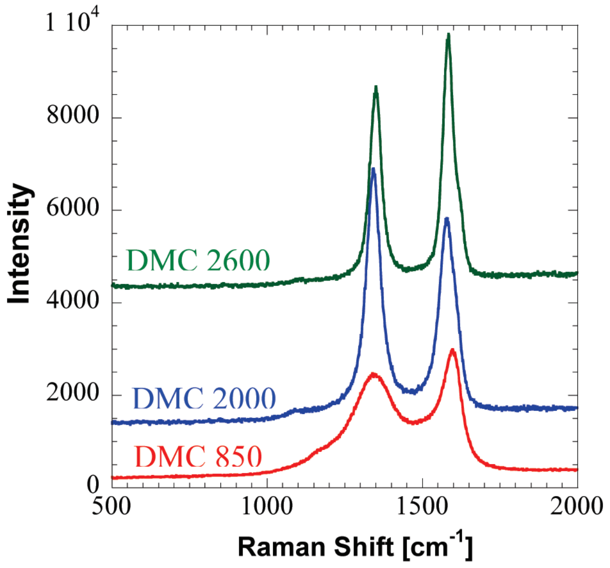

Figure 2. Raman spectra of the disordered mesoporous carbons annealed at different temperatures.

The G band is present in all sp^2 hybridized carbon materials and arises from the E_{2g} vibrational mode. By determining the area under the peak for the D band and the G band, I_D/I_G (ratio of amorphous to graphitic character) values were estimated and decreased monotonically as 1.30, 1.24, and 1.02 for DMC-850, 2000, and 2600, respectively. The decreasing I_D/I_G with increasing carbon temperature is indicative of improving degree of graphitization. The relative levels of graphitization can be discerned by estimating the in plane crystalline length, L_a ($= 4.4/(I_d/I_g)$)[55] in nanometers. As the I_D/I_G ratio decreases, L_a increases ($L_a = 3.38$, 3.74, 4.32 nm for DMC 850, 2000, and 2600, respectively) as graphitic crystallites grew in size with increasing carbon treatment temperature. These L_a values are in good agreement to those estimated from XRD data (see Table 1).

Nanoparticles with two different compositions were synthesized by starting with Pt:Cu molar precursor ratios of 25:75 and 50:50, which led to similar final compositions of $Pt_{20}Cu_{80}$ and $Pt_{45}Cu_{55}$ respectively, as determined using SEM-EDS. For DMC-850 and DMC-2000, loadings of 17% and 8%, respectively, were achieved for a starting concentration of 20 mg/mL of $Pt_{20}Cu_{80}$ (Table 2). To achieve a loading of 14% for $Pt_{20}Cu_{80}$ in the more graphitic DMC-2000, the initial concentration of nanoparticles was increased to 30 mg/mL and the time of infusion was raised to 5 days. In contrast, for amorphous Vulcan XC-72, almost all the $Pt_{20}Cu_{80}$ nanoparticles were adsorbed in a relatively short time span of 2 days and at a low starting concentration of 5 mg/mL, suggesting that the surface oxygen sites on the amorphous carbon facilitated adsorption.

The Pt−Cu nanoparticles were electrochemically dealloyed to leach off copper selectively from the nanoparticle surface to produce a highly active strained Pt surface.[1,17,56] Figures 3 and Figure S4 in the Supporting Information show cyclic voltammograms for $Pt_{20}Cu_{80}$/SDC-2000 catalyst for slow potential cycling between 0.04 and 1.24 at 20 mV/s. The first dealloying cycle does not show a characteristic anodic stripping peak between 0.04 and 0.4 V, associated with underpotentially deposited hydrogen on platinum surfaces. Here, the Cu-rich surface of the Pt−Cu nanoparticles contains very little Pt. This result is consistent with the segregation of the copper to the surface in Cu-rich Pt−Cu alloys, given its lower surface energy.[57] A broad anodic peak appeared at 0.3 V and extended almost to 0.85 V, indicating Cu dissolution. After 3 dealloying cycles, two distinct copper dissolution peaks at 0.3 and 0.7 V emerge. With further cycles, the peak intensity and area of copper dissolution peaks decrease as the surface becomes enriched with Pt, indicated by the appearance and growth of an anodic

---

(55) Tuinstra, F.; Koenig, J. L. *J. Chem. Phys.* **1970**, *53*(3), 1126–30.

(56) Strasser, P.; Koh, S.; Greeley, J. *Phys. Chem. Chem. Phys.* **2008**, *10* (25), 3670–3683.

(57) Ruban, A. V.; Skriver, H. L.; Norskov, J. K. *Phys. Rev. B: Condens. Matter Mater. Phys.* **1999**, *59*(24), 15990–16000.

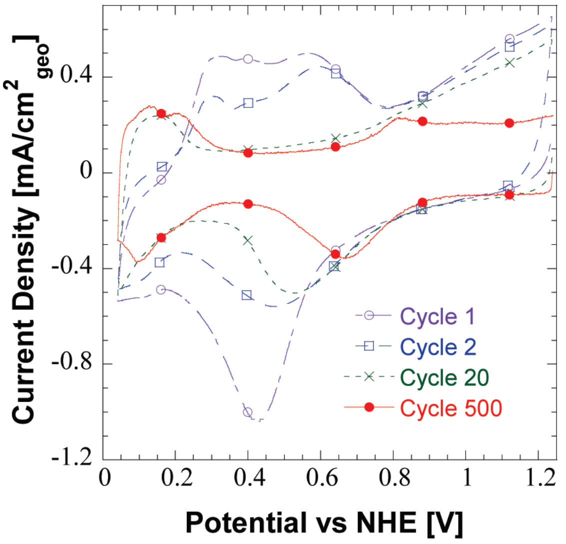

Figure 3. Cyclic voltammetry of $Pt_{20}Cu_{80}$ nanoparticles supported on DMC-2000 during electrochemical dealloying at 20 mV/s under an argon atmosphere.

hydrogen desorption peak between 0.04 and 0.4 V. After about 500 cycles, the cyclic voltammograms reach a steady state or equilibrium behavior with the signature of a nearly pure Pt surface (see Figure S5 in the Supporting Information), with the familiar hydrogen ad/desorption range (0.05−0.4 V) as well as the Pt oxide formation and desorption peaks at 0.83 and 0.72 V on the anodic and cathodic scan, respectively.

The dealloying mechanism changes significantly upon progressive Cu removal. After just 20 dealloying cycles, copper dissolution peaks at 0.3 V and 0.7 V essentially disappear, as the surface becomes composed of almost pure Pt. However, the "strongly" and "weakly" bound hydrogen desorption peaks associated with Pt ⟨100⟩ and ⟨111⟩ respectively, are not present, indicating an amorphous structure.[58] After the completion of 500 dealloying cycles, these peaks become present at 0.16 and 0.21 V (Figure 3), indicating crystalline platinum.[59] Thus, while the initial dealloying cycles facilitate Cu removal from the surface, the subsequent dealloying cycles facilitate the structural reordering of the platinum atoms upon crystallization.

Figure 4(a) shows XRD spectra of the $Pt_{20}Cu_{80}$/DMC-2000 before and after dealloying. Before dealloying, the ⟨111⟩ peak approaching that of pure copper is present. The peaks at 43.1, 69, and 83.1° are associated with the ⟨111⟩, ⟨220⟩, and ⟨311⟩ crystal planes of FCC lattice. The phases of the nanocrystal were investigated by peak fitting using JADE software, as shown in Figure 4b and Table 3. A Cu-rich alloy phase with a peak at 42.7° was present, along with a small Pt-rich phase as indicated by the peak at 40.1°. From the relative areas, the Cu-rich phase was ~95% with only about ~5% of a Pt-rich phase. The peak position can be used to determine the phase compositions with Vegard's Law[60,61] The composition of the FCC-disordered Pt−Cu alloy can be estimated from observed unit cell parameters according to $a_c = a_0 - kx_{Cu}$, where $a_0 = 3.923$ Å is the unit-cell parameter of pure Pt, a_c is the measured cell parameter of a Pt−Cu alloy, x_{Cu} is the molar ratio of Cu in the binary alloys, and k is a constant (~0.308 Å for the Pt−Cu system).[62] The unit-cell

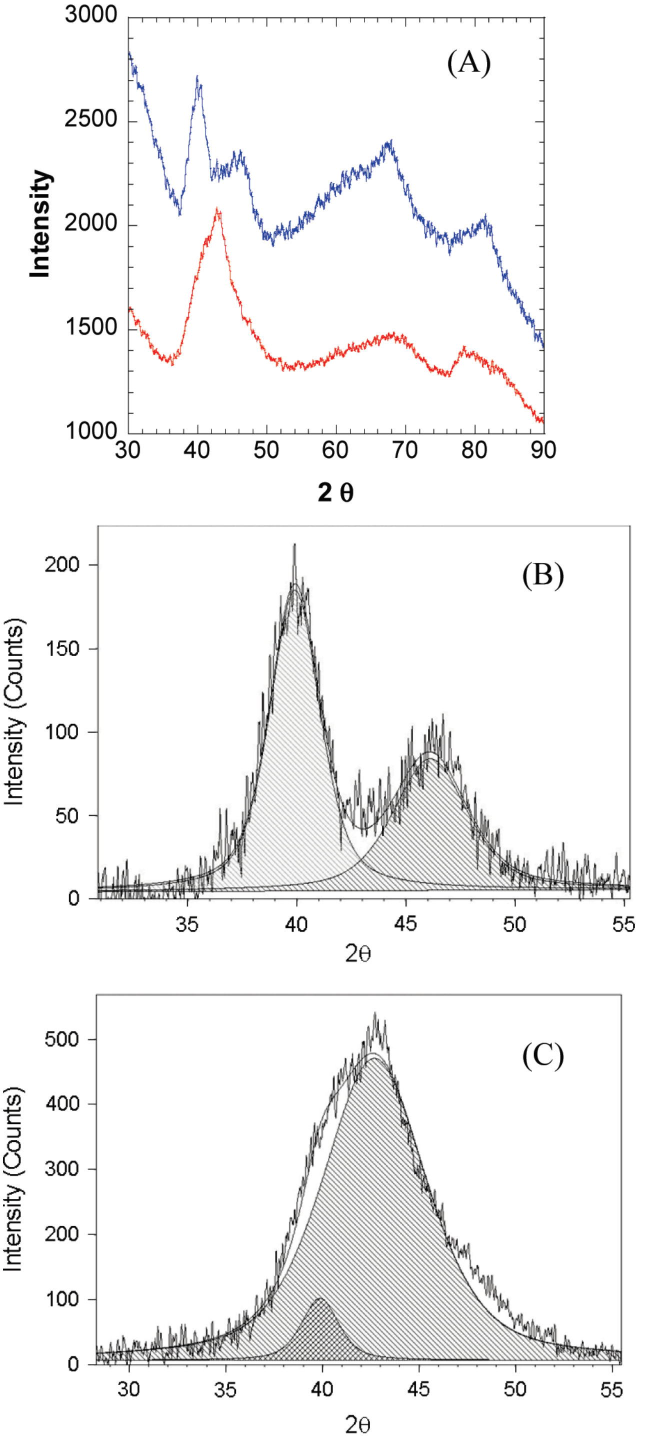

Figure 4. XRD spectra of (a) 14% $Pt_{20}Cu_{80}$ nanocrystals supported on DMC-2000 before and after electrochemical dealloying of copper, (b) peak analysis of the XRD spectra of the as-synthesized $Pt_{20}Cu_{80}$ nanoparticles, (c) and electrochemically dealloyed nanoparticles with a final composition of $Pt_{85}Cu_{15}$.

---

(58) Mukerjee, S. *J. Appl. Electrochem.* **1990**, *20*(4), 537–48.
(59) Kinoshita, K. *J. Electrochem. Soc.* **1990**, *137*(3), 845–8.
(60) Vegard, L. *Z. Phys.* **1921**, *5*, 393–5.
(61) Vegard, L. *Z. Phys.* **1921**, *5*, 17–26.
(62) Liu, Z.; Koh, S.; Yu, C.; Strasser, P. *J. Electrochem. Soc.* **2007**, *154* (11), B1192–B1199.

Table 3. Composition and Structural Analysis of 14% $Pt_{20}Cu_{80}$/DMC-2000 before and after Dealloying

catalyst	D_{TEM} (nm)	D_{XRD} (nm)	CSA_{TEM} (m^2/g)	CSA_{XRD} (m^2/g)	SEM-EDS composition	Bravais lattice	lattice parameter (Å)	composition (Vegard's law)	ratio of 111 peak areas
before dealloying	3.25	3.0	86	93	$Pt_{20}Cu_{80}$	FCC1	3.663	$Pt_{17}Cu_{83}$	FCC1: FCC2 = 19:1
						FCC2	3.881	$Pt_{90}Cu_{10}$	
after dealloying	2.95	2.7	95	100	$Pt_{85}Cu_{15}$	FCC	3.876	$Pt_{85}Cu_{15}$[a]	

[a] Vegard's law was used only as an estimate here because the particles after dealloying are strained and not a regular FCC substitutional solid.

parameter a_c for the Pt−Cu alloy can be related to the lattice spacing for ⟨111⟩ peak and 2θ according to

$$d_{111}^{Pt-Cu} = a_c/\sqrt{3}$$
$$\lambda = 2d_{111}^{Pt-Cu} sin(\theta) \qquad (1)$$

The composition of the copper-rich phase was $Pt_{17}Cu_{83}$, in agreement with SEM-EDS, whereas that of the platinum-rich phase was $\sim Pt_{90}Cu_{10}$. The nanoparticle size was estimated to be 3.0 nm from the Scherrer equation.

After dealloying, the ⟨111⟩ peak shifts to lower 2θ values relative to the ⟨111⟩ peak before dealloying, as copper is leached from the nanoparticle surface (Figure 4a). After dealloying four peaks appear at 40.54°, 46.74, 68.4, and 81.26°, corresponding to the ⟨111⟩, ⟨200⟩, ⟨220⟩, and ⟨311⟩ FCC crystal planes, respectively. As shown in Figure 4c, only one platinum-rich alloy phase was present in the dealloyed nanoparticles. The composition was estimated to be $Pt_{85}Cu_{15}$ using Vegard's law (Table 3). Though Vegard's law is based on unstrained particles, it provides a rough estimate for strained particles. We found the results of the law to be in good agreement with the area-averaged composition of $Pt_{82}Cu_{18}$ determined from SEM-EDS. The nanocrystal size after dealloying from the Scherrer equation was 2.8 nm, indicating a 10% reduction after dealloying.

Figure 5 shows TEM micrographs and histograms of $Pt_{20}Cu_{80}$ on DMC-2000 before and after electrochemical dealloying. The nanoparticles are well-dispersed on the support with little aggregation upon ligand removal or during the dealloying process. The average nanoparticle diameter increases slightly from 2.85 nm (see Figure S2 in the Supporting Information) to 3.25 nm (panels A and C in Figure 5) upon thermal calcination for ligand removal. It decreased from 3.25 to 2.95 nm upon dealloying (Table 3, panels B and D in Figure 5) in good agreement with the sizes from XRD. The difference in the TEM and XRD diameters is within the experimental uncertainty in the XRD values. Images E and F in Figure 5 show high-resolution images of PtCu nanoparticles on DMC 2000 before and after dealloying, respectively. The composition for this sample was determined via EDS to be $Pt_{50}Cu_{50}$, which was dealloyed to $Pt_{75}Cu_{25}$. The lattice fringes can been seen on each image, demonstrating crystallinity. Particles sizes for this sample were ~3 nm, similar to that of $Pt_{20}Cu_{80}$. The chemical surface area (CSA) after dealloying was determined from XRD and TEM particle sizes ($CSA = 3/(\rho_{Pt} r_{np})$) to be ~95−100 m^2/g for $Pt_{20}Cu_{80}$ (Table 3).

Activity and Stability of the Pt−Cu Catalysts toward Oxygen Reduction Reaction. The electrochemical surface area ($ECSA = Q_H/(m_{pt}c)$] of the platinum-enriched nanoparticles after dealloying was estimated from the area of the anodic hydrogen desorption peak between 0.04 and 0.4 V,[63] where Q_H is the charge for desorption (mC), m_{pt} is the mass of platinum on the electrode, and c is a constant defined by the charge required to oxidize a monolayer of hydrogen on Pt (0.21 mC/cm^2). The catalysts in this paper are compared to commercially available 20% Pt on Vulcan carbon (ETEK) tested at 80 °C.[64] The estimated ECSA for 14% $Pt_{20}Cu_{80}$ on DMC-2000 was 83 $m^2/g_{Pt,}$ slightly better than that of the commercial catalyst. The ECSA was ~85% of the chemical surface area estimated by XRD and TEM (Table 3), indicating 85% of the total Pt sites are electrochemically accessible.

Figure 6 shows the cyclic voltammograms of the dealloyed $Pt_{80}Cu_{20}$ on DMC-2000 before and after ADT cycling. The cyclic voltammograms show two peaks in the underpotentially deposited hydrogen region between 0.05 and 0.3 V associated with the weak and strong desorption of hydrogen. The multiple crystal facets present on the crystalline dealloyed $Pt_{80}Cu_{20}$ nanoparticles bind with hydrogen with varying strength and hence lead to two desorption peaks. After ADT cycling between potentials of 0.5 V and 1.2 V for 1000 cycles, the area under the hydrogen desorption peak remains virtually unchanged, indicating negligible loss in platinum area due to sintering, coalescence, Pt dissolution, or Ostwald ripening.

Figure 7 shows a representative linear scan voltammogram obtained for the oxygen reduction reaction with dealloyed Pt−Cu/DMC-2000. The diffusion-limited current densities were 6.3, 6.0, and 5.6 mA/cm^2 for $Pt_{20}Cu_{80}$/DMC-2000, $Pt_{20}Cu_{80}$/DMC-850, and $Pt_{45}Cu_{55}$/DMC-2000, respectively. These results are similar to the value for a smooth polycrystalline Pt-disk electrode (6 mA/cm^2).

Figure 8 shows the Tafel slopes for the dealloyed $Pt_{20}Cu_{80}$ on DMC-2000 and DMC-850 catalysts, in the kinetically controlled regime relative to a commercial platinum catalyst. Both the mass and surface activities for the dealloyed $Pt_{20}Cu_{80}$ are significantly better than those of the commercial Pt catalyst, as seen in previous studies with similar Pt−Cu composition.[1,13]

---

(63) Chen, Z.; Deng, W.; Wang, X.; Yan, Y. *ECS Trans.* **2007**, *11*(1, Part 2, Proton Exchange Membrane Fuel Cells 7, Part 2), 1289–1299.

(64) Gasteiger, H. A.; Kocha, S. S.; Sompalli, B.; Wagner, F. T. *Appl. Catal., B* **2005**, *56*(1−2), 9–35.

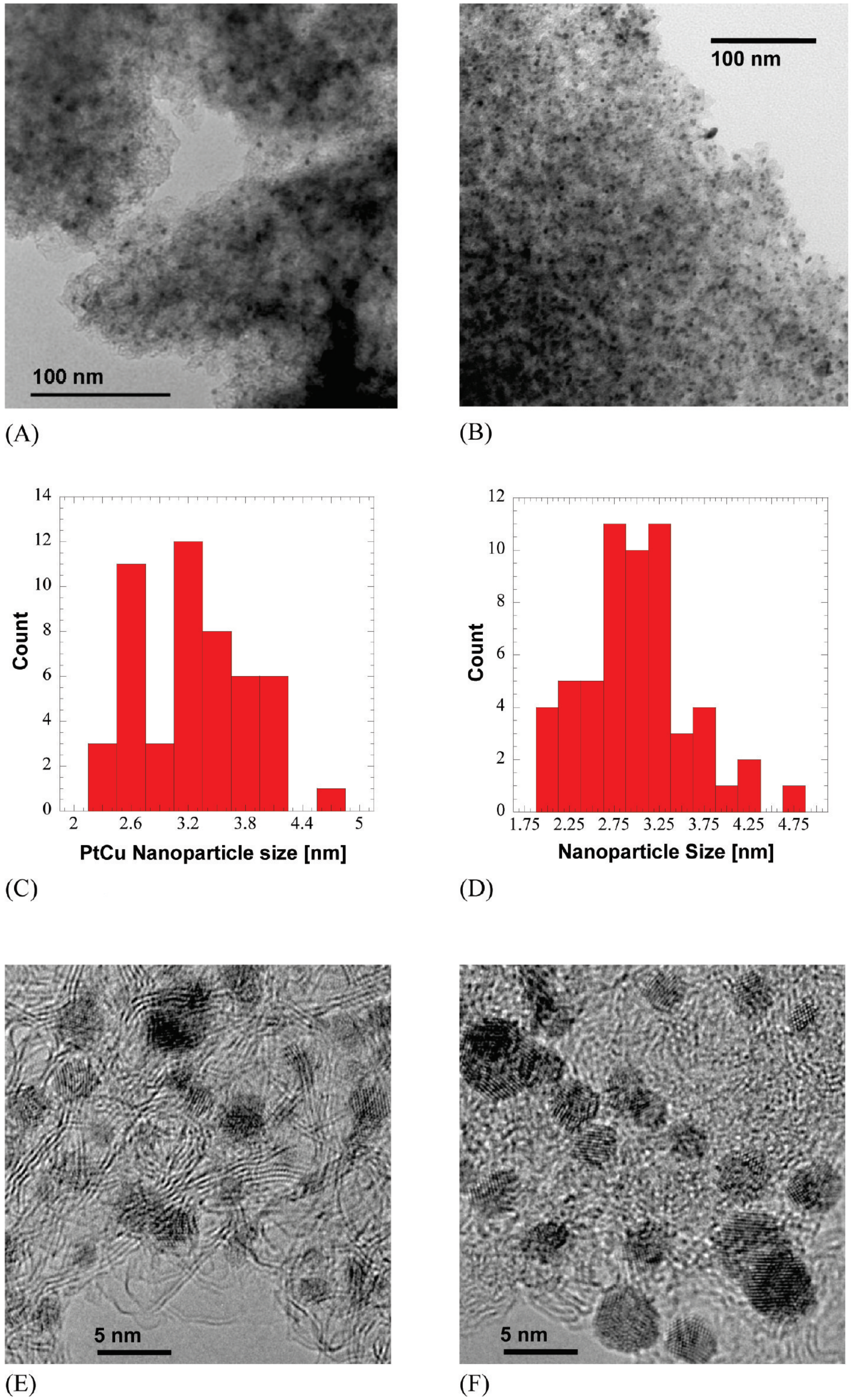

Figure 5. TEM micrographs and histograms of $Pt_{20}Cu_{80}$ on DMC-2000 (A, C) as-synthesized and (B, D) calcined at 350 °C and electrochemically dealloyed. Average nanoparticle size changed from 3.25 to 2.95 nm after dealloying. Histograms generated from larger image (only a portion of micrograph shown). (E, F) High-resolution images showing lattice fringes of $\sim Pt_{50}Cu_{50}$ on SDC 2000 before and after dealloying, respectively.

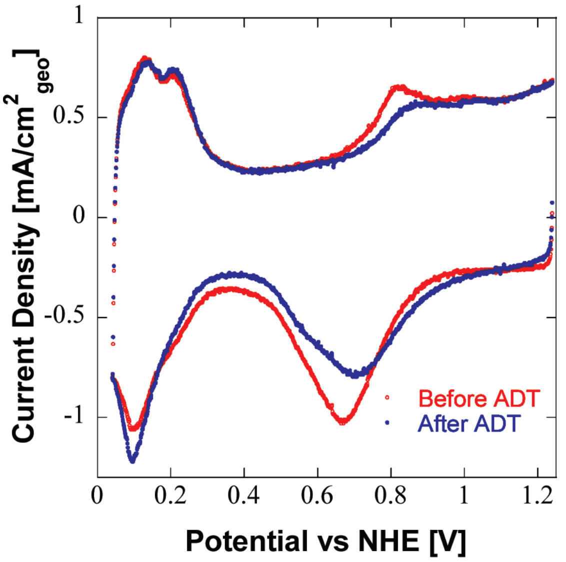

Figure 6. Cycling voltammograms for $Pt_{20}Cu_{80}$ on DMC 2000 before and after ADT potential cycling.

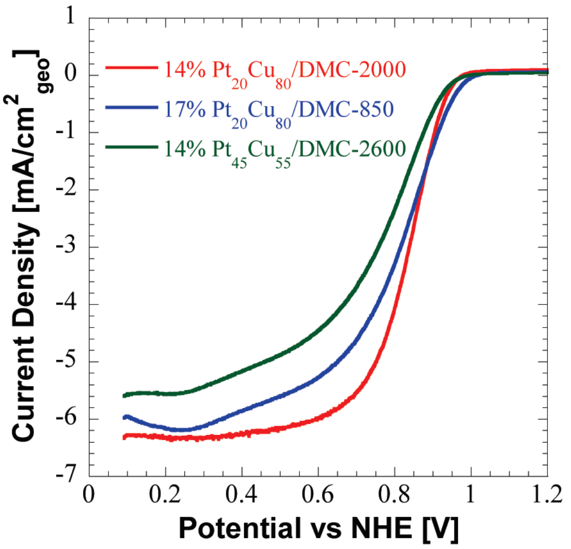

Figure 7. Linear scan voltammetry of the dealloyed Pt−Cu nanoparticles supported on DMC at 5 mV/s with a rotation rate of 1600 rpm.

The electrochemical properties are reported in Table 4 at 0.9 V, a value of interest for fuel cells.[64] The values of 0.41−0.46 A/mg Pt for dealloyed $Pt_{20}Cu_{80}$ on DMC-850 and DMC-2000, as well as on Vulcan XC72 was ~ 4 times larger than for the commercial catalyst.[64] The mass activities before ADT were not influenced significantly by the degree of graphitization. Similarly, the area activities were more than three times greater than that of the commercial Pt catalyst. The mass activity was only 0.23 for $Pt_{45}Cu_{55}$ supported on DMC-2600. For $Pt_{45}Cu_{55}$, less Cu is removed during dealloying leading to a smaller activity enhancement as seen previously.[65]

The activities of the catalysts were also measured after ADT cycling (Figure 8 and Table 4). For the two significantly amorphous carbons, DMC-850 and the commercial Vulcan carbon, a significant loss in mass activity and ECSA was observed. Loses on the order of 20−70% during similar potential cycling experiments are nearly always observed in the literature for similar types of significantly amorphous C.[6,25] However, for the three experiments with highly graphitic carbons, DMC 2000 and 2600, the mass and area activities as well as the ECSAs were remarkably stable during ADT. Enhanced stability has been observed recently for pure Pt on graphitic mesoporous carbon treated at 2600 °C.[31] To the best of our knowledge, this type of stability has not been reported previously for bimetallic catalysts for the ORR.

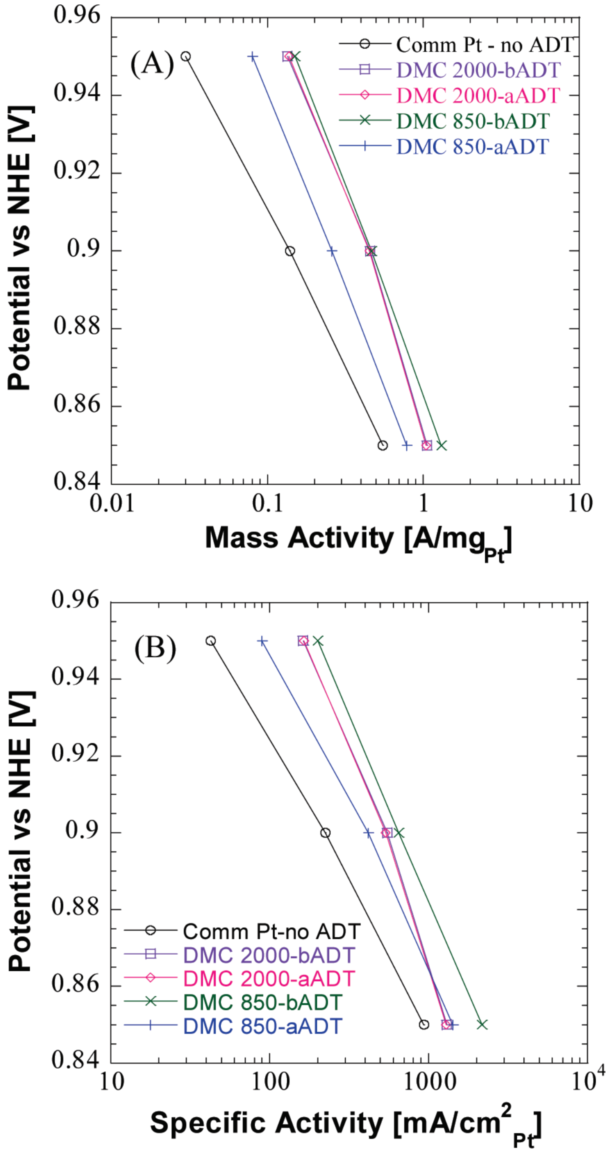

Figure 8. Potential−activity plots of dealloyed $Pt_{20}Cu_{80}$ nanoparticles supported on DMC-2000 and DMC-850 compared to commercial Pt (ETEK) catalysts: (a) Pt mass-based activities and (b) Pt specific surface area activities.

Discussion

Carbon Oxidation and Impact on Stability. For Pt−Cu supported on the DMC-850 support, a significant loss in activity was observed upon ADT potential cycling.

---

[65] Koh, S.; Hahn, N.; Yu, C.; Strasser, P. *J. Electrochem. Soc.* **2008**, *155*(12), B1281–B1288.

Table 4. Activity and Stability during an Accelerated Durability Test (ADT, 1000 cycles from 0.5 to 1.2 V) of Dealloyed Pt−Cu Catalysts Supported on Mesoporous Carbons

composition	I (A/mg Pt) before ADT[a]	I (μA/cm^2) before ADT[a]	ECSA before ADT (m^2/g Pt)	I (A/mg Pt) after ADT[a]	I (μA/cm^2) after ADT[a]	ECSA after ADT (m^2/g Pt)
17% Pt$_{20}$Cu$_{80}$/DMC-850	0.46	630	73	0.27	435	62
14% Pt$_{20}$Cu$_{80}$/DMC-2000	0.45	537	83	0.45	540	84
15% Pt$_{20}$Cu$_{80}$/DMC-2000	0.41	471	82	0.41	474	83
14% Pt$_{45}$Cu$_{55}$- DMC-2600	0.23	382	59	0.22	332	66
20% Pt$_{20}$Cu$_{80}$/vulcan-XC72	0.42	495	68	0.20	198	38

[a] All activities are calculated at 0.9 V.

DMC-850 is amorphous in nature as shown by XRD and Raman spectroscopy in Figures 1 and 2. It is oxidized when subjected to potentials ≥1.2 V in highly corrosive acidic environments as reported previously for other amorphous carbons.[29,66] The surface oxygen species on the amorphous carbon acts as reactive centers and accelerate carbon oxidation.[28,32] Pt atoms on the carbon surface (after dealloying Pt−Cu) catalyze the carbon oxidation.[67] We found that 20% Pt on amorphous Vulcan XC-72 lost about 9% of its weight under isothermal conditions of 195 °C in 16 days because of carbon loss. Degradation of carbon leads to metal nanoparticle isolation and partly contributes to activity losses during ADT potential cycling (Figure 8).

The support degradation and consequent activity loss were alleviated by graphitization of the carbon support as seen for DMC-2000 and 2600 (Table 4).[66] The graphitic character of DMC-2000 can be seen in Figure 1B by the significant number of graphitic ribbons. The high temperature graphitization reduces the number of surface oxygen functionalities and thus increases the resistance to oxidation.[29] For example, the onset temperature for 20% Pt on graphitized DMC-2000 is ~ 180 °C higher than for 20% Pt on amorphous DMC-850 (as seen by TGA, Figure S7 in the Supporting Information) indicating significantly higher oxidation resistance. The weight loss of carbon for 20% platinum on the more graphitic carbons under isothermal conditions at 195 °C for 16 days was insignificant, (<0.7 wt %, which is within the error limit) also indicating high oxidation resistance (see Figure S8 in the Supporting Information). The resistance to electrochemical oxidation of the graphitized mesoporous carbons during ADT is further indicated in Table 4 by the small losses in ECSA and ORR activity.

Metal−support Interactions in Graphitic Carbon and Their Impact on Catalyst Synthesis and Stability. The high metal loadings of Pt−Cu nanoparticles infused into the graphitized DMC-2000 and DMC-2600 were facilitated by the short-ranged interactions between the metal and the support, as shown previously for metals on silica supports.[41] The surface of the Pt$_{20}$Cu$_{80}$ nanoparticles is Cu-rich, as observed from the initial dealloying curves (Figure 3). Relatively strong interactions between Cu and graphitic fullerene due to charge transfer from Cu to fullerene have been identified with high frequency Raman spectra.[45] The peak width of the pentagon-pinch mode becomes wider and the peak position shifts to the lower frequency as the atomic ratio of Cu/C increases, indicating strong metal−support interactions. These short-ranged interactions enable the adsorption of Cu-rich Pt−Cu nanoparticles on the mesoporous carbon supports to render high loadings (Table 2).

To achieve high nanoparticle loadings, the short-ranged interactions of the metal surfaces with the support must not be screened too strongly by the hydrocarbon capping ligands. The strategic selection of the relatively weakly binding oleic acid/oleyl amine ligands with low surface coverage (wt of ligand on Pt−Cu was 20% as determined from TGA), exposes enough bare metal to facilitate strong metal(primarily Cu)−support interactions.[41,68,69] These short-ranged interactions are further strengthened by the favorable geometric contact area between the convex nanoparticles and the concave mesopores.[41,36] The ligands were removed at a relatively low temperature of 350 °C, without causing any significant nanoparticle sintering. After dealloying, the Pt nanoparticle surface binds very strongly with the graphitized carbons, as indicated by the shifting of the binding energy for the Pt 4f$_{7/2}$ peak to higher energy value (refer to XPS data in Figure S6 of the Supporting Information) compared to both unsupported Pt and Pt on amorphous carbon.[70,71] The exact nature of the Pt interaction with graphite is still a topic of considerable discussion. However, it is reported that the delocalized electrons in the p-orbital of the π sites on graphite overlap with the d-orbital of the Pt, indicating that the nature of the binding is partially covalent.[30] In addition, partial electron transfer from the Pt to the graphitic surface has also been determined by previous XPS[30] and DFT[72] studies. Thus, the strong partially covalent bond due to orbital overlap coupled with partial charge transfer between Pt and graphitic surfaces enables strong metal−support interactions and thus facilitates high catalyst stability (Table 4).

---

(66) Mathias, M. F.; Makharia, R.; Gasteiger, H. A.; Conley, J. J.; Fuller, T. J.; Gittleman, C. I.; Kocha, S. S.; Miller, D. P.; Mittelsteadt, C. K.; Xie, T.; Yan, S. G.; Yu, P. T. *Electrochem. Soc. Interface* **2005**, *14*(3), 24–35.

(67) Stevens, D. A.; Hicks, M. T.; Haugen, G. M.; Dahn, J. R. *J. Electrochem. Soc.* **2005**, *152*(12), A2309–A2315.

(68) Jana, N. R.; Peng, X. *J. Am. Chem. Soc.* **2003**, *125*(47), 14280–14281.

(69) Yu, R.; Song, H.; Zhang, X.-F.; Yang, P. *J. Phys. Chem. B* **2005**, *109*(15), 6940–6943.

(70) Fu, X.; Wang, Y.; Wu, N.; Gui, L.; Tang, Y. *J. Colloid Interface Sci.* **2001**, *243*(2), 326–330.

(71) Antolini, E.; Giorgi, L.; Cardellini, F.; Passalacqua, E. *J. Solid State Electrochem.* **2001**, *5*(2), 131–140.

(72) Yang, D. Q.; Zhang, G. X.; Sacher, E.; Jose-Yacaman, M.; Elizondo, N. *J. Phys. Chem. B* **2006**, *110*(16), 8348–8356.

The metal−support interactions prevent the coalescence of dealloyed Pt nanoparticles during stability cycling, consistent with no loss in electrochemical surface area after ADT (Figure 8), typically observed for amorphous carbons.[24] Similar beneficial effect of strong Pt−graphite interactions for preventing coalescence of Pt nanoparticles at high temperatures has been reported by Coloma et al.[27]

The stability in ECSA, CSA, and ORR activity for the dealloyed Pt−Cu on DMC-2000 and DMC-2600 suggest insignificant Pt dissolution and/or subsequent Ostwald ripening as a result of the resistances of the carbons to oxidation and of the promotion of strong catalyst−support interactions. The relatively monodisperse size of the dealloyed particles further limits Ostwald ripening. The larger size of the PtCu particles (∼3 nm) compared to the smaller Pt particles on Vulcan carbon (∼2 nm) could also play a role in the enhanced stability, as has been observed elsewhere.[73] Although, the effect of metal−support interactions on Pt dissolution is not well studied, it is plausible that the C−Pt binding synergistically alters the electronic structure of the Pt, causing the observed shift to higher binding energies for the Pt $4f_{7/2}$ XPS spectra (see Figure S6 in the Supporting Information), thereby creating a stabilizing effect against Pt oxidation. The delocalization of electron density in the orbital overlap between the Pt and the π sites on the carbon lowers the tendency to form a Pt−O bond as the potential becomes more positive, resulting in a decrease in Pt dissolution. A related method to alter the Pt electronic structure to make it less resistant to dissolution is galvanic deposition of Au clusters on Pt nanoparticles.[21]

The geometry of the mesopores in the carbon helps to bolster the stability as well. The large interfacial contact area between the nanoparticles and concave mesopores with relatively similar radii will strengthen metal−support interactions. In PEM fuel cells, the large 3D disordered mesopores will facilitate accessibility of the reactant gas and polymer electrolyte relative to other types of carbons with inaccessible micropores.

The dealloying cycles to remove Cu may also cause some Pt dissolution. The upper potential in the ADT of 1.2 V is slightly less than the value of 1.24 V in the dealloying cycles. However, the value of the lower potential is significantly smaller for the dealloying cycles (0.05 V compared to 0.51 V for ADT). The lower potential limit of 0.05 V allows for the reduction Pt oxides back to Pt, and thus causes less Pt dissolution than in the case of the ADT cycles.

High loadings of bimetallic catalysts on carbon with controlled compositions and size are difficult to achieve with traditional precursor reduction techniques such as wet impregnation, particularly for graphitic carbons. The lack of polar and charged oxygenated sites on the graphitic surface precludes strong ion-dipole and electrostatic interactions with ionic metal precursors.[28] Consequently, the weakly interacting metal precursors often lead to undesirably large nanoparticle sizes (>5 nm) upon reduction.[28] To enhance precursor interactions, the graphitic carbons may be oxygenated with acids.[22] However, these oxygen groups weaken the interactions of the final metal nanoparticles with graphitic π electrons and make the carbon more susceptible to oxidation in fuel cells.

Dealloying−Catalyst Structure and Activity Enhancement for Particles with Essentially One Alloy Phase. The straining of the Pt shell from the underlying Cu in the dealloyed nanoparticles has been shown to raise the catalyst activity markedly.[1,13] It has been shown experimentally and theoretically that the selective dissolution of Cu from the nanoparticle creates a strain Pt-rich surface.[17,56] However, it is challenging to understand the effect of strain for bimetallic particles with multiple Pt−Cu phases, as are typically produced by traditional precursor reduction techniques including wetness-impregnation.[1,13,34,74](see the Supporting Information for further details). In contrast, the very small amounts of secondary phases for the particles in the present study, both before and after dealloying (Figure 4), are beneficial for elucidating effect of particle morphology on activity and, ultimately, for optimizing catalyst activity.

Both pure platinum and copper exhibit an FCC crystal structure which is favorable for forming predominantly a single phase. The precursor concentrations were tuned to control nucleation and growth rates to focus the nanocrystal size and composition. The precursors were reduced simultaneously in absence of the carbon supports, which may otherwise cause heterogeneous nucleation of multiple phases.[1,13,34,74] The essentially single-phase Cu-rich particles synthesized via arrested growth precipitation were dealloyed to a single-phase Pt-rich alloy. The copper apparently leached out at similar rates from particle to particle because the starting catalyst was not composed of many phases.

The dealloying of the $Pt_{20}Cu_{80}$ nanoparticles to $Pt_{85}Cu_{15}$ results in an almost pure Pt surface with a copper-enriched core (Figure 3 and Figures S4 and S5 in the Supporting Information) as previously hypothesized by Strasser and others.[1] A smaller lattice parameter was observed for the Pt-rich particles after dealloying relative to pure Pt nanoparticles (Table 3). Thus, the strain from the copper core reduced Pt−Pt distances on the particle surface and enhanced the activity.

Conclusions

Herein, we have designed highly stable and highly active bimetallic Pt−Cu catalysts on graphitized mesoporous carbon with a presynthesis/infusion technique. The unprecedented stability of these highly graphitic bimetallic ORR catalysts is indicated by a negligible loss in ECSA as well as catalytic activity ($<2\%$ for both) after 1000 cycles between 0.5 V and 1.2 V. Typically a 70% loss is observed for a typical commercial carbon (Vulcan XC-

---

[73] Makharia, R.; Kocha, S. S.; Yu, P. T.; Sweikart, M. A.; Gu, W.; Wagner, F. T.; Gasteiger, H. A. *ECS Trans.* **2006**, *1*(8, Durability and Reliability of Low-Temperature Fuel Cells Systems), 3–18.

[74] Fernandez, J. L.; Raghuveer, V.; Manthiram, A.; Bard, A. J. *J. Am. Chem. Soc.* **2005**, *127*(38), 13100–13101.

72). The oxidation resistance of the highly graphitic supports, which contain very few surface oxygen sites, prevents nanoparticle isolation from the surface. The strong covalent and charge-transfer interactions between the π electrons on the graphitic carbon surface and the enriched Pt surface of the dealloyed nanoparticles mitigate sintering, Pt dissolution. and Ostwald ripening. The metal–carbon interactions are further enhanced by the large interfacial contact area between the metal nanocrystals and concave mesopores with relatively similar radii. Removal of 90% of the copper from these nanoparticles via dealloying produced single-phased $Pt_{85}Cu_{15}$ particles with large strain in their Pt shells, resulting in a 4-fold activity enhancement for ORR over pure Pt nanoparticles, as reported previously for Vulcan XC-72 carbon.[1] The arrested growth precipitation of Pt–Cu nanoparticles with stabilizing ligands favors focusing of the size (< 3 nm) as well as the composition, as shown by TEM and XRD both before and after dealloying. The ability to design and control the size and composition of bimetallic nanocrystals is beneficial for tuning catalyst activity and stability. Catalysts with well-defined architectures will guide fundamental understanding of catalytic mechanisms. This understanding will be useful for future design of highly active and stable catalysts, including electrocatalysts for oxygen reduction in PEM fuel cells.

Acknowledgment. This material is based on work supported in part by the STC Program of the National Science Foundation under Agreement CHE-9876674, the Department of Energy Office of Basic Energy Sciences, and the Robert A. Welch Foundation (F-1319 and F-1529).

Supporting Information Available: Nitrogen porisometry and TGA and UV–vis data for metal weight percent loadings as well as additional characterization via TEM, XRD, XPS, and electrochemical methods (PDF). This material is available free of charge via the Internet at http://pubs.acs.org.